
Validating Conditional Density Models and Bayesian Inference Algorithms

David Zhao¹

Niccolò Dalmaso¹

Rafael Izbicki²

Ann B. Lee¹

¹Department of Statistics & Data Science, Carnegie Mellon University, Pittsburgh, Pennsylvania, USA

²Department of Statistics, Federal University of São Carlos (UFSCar), São Carlos, Brazil

Abstract

Conditional density models $f(y|\mathbf{x})$, where \mathbf{x} represents a potentially high-dimensional feature vector, are an integral part of uncertainty quantification in prediction and Bayesian inference. However, such models can be difficult to calibrate. While existing validation techniques can determine whether an approximated conditional density is compatible overall with a data sample, they lack practical procedures for identifying, localizing, and interpreting the nature of (statistically significant) discrepancies over the entire feature space. In this paper, we present more discerning diagnostics such as (i) the “Local Coverage Test” (LCT), which is able to distinguish an arbitrarily misspecified model from the true conditional density of the sample, and (ii) “Amortized Local P-P plots” (ALP) which can quickly provide interpretable graphical summaries of distributional differences at any location \mathbf{x} in the feature space. Our validation procedures scale to high dimensions, and can potentially adapt to any type of data at hand. We demonstrate the effectiveness of LCT and ALP through a simulated experiment and a realistic application to parameter inference for galaxy images.

quantifies uncertainty about the parameters θ of interest after observing data \mathbf{x} . Often the posterior f is not tractable, so computational methods such as Markov Chain Monte Carlo [Brooks et al., 2011] are used to produce samples from an approximation of f at the observed value of \mathbf{x} .

Recently, a large body of work in machine learning has been developed for estimating conditional densities f for all possible values of \mathbf{x} (see Uria et al. 2014, Sohn et al. 2015, Papamakarios et al. 2017, Dutordoir et al. 2018 and references therein). With the advent of high-precision data and simulations, simulation-based inference (SBI; Cranmer et al. [2020]) has also played a growing role in disciplines ranging from physics, chemistry and engineering to the biological and social sciences. The latter SBI category includes both classical MCMC-based methods for approximating posteriors (e.g., ABC; Sisson et al. [2018]), as well as machine-learning based methods to learn an explicit surrogate model of the posterior [Marin et al., 2016, Papamakarios and Murray, 2016, Lueckmann et al., 2017, Chen and Gutmann, 2019, izb, 2019, Greenberg et al., 2019].

Inevitably, any downstream analysis in Bayesian inference or predictive modeling will depend on the trustworthiness of the assumed conditional density model. Validating such models can be challenging, especially for a high-dimensional feature vector or mixed-type data \mathbf{x} . To date, we do not have a comprehensive and rigorous process of testing, for all possible values of \mathbf{x} , whether a conditional density model $\hat{f}(y|\mathbf{x})$ fits actually observed data, or equivalently (in the Bayesian framework) if an approximation $\hat{f}(\theta|\mathbf{x})$ of the posterior fits the true posterior given by the model.

In machine learning, validation and model selection typically rely on a global loss function like the Kullback-Leibler divergence or the L^2 loss [Izbicki et al., 2017a, Rothfuss et al., 2019]. Loss functions are useful for training models, but they only provide relative comparisons of overall model fit. Hence, a practitioner may not know whether he or she should keep looking for better models (using larger training samples, training times, etc.), or if the current estimate is

1 INTRODUCTION

Conditional densities models play a key role in uncertainty quantification. For instance, the conditional density $f(y|\mathbf{x})$ of the response variable y given features \mathbf{x} can be used to build predictive regions for y , which are more informative than point predictions. Indeed, in prediction problems, f provides a full account of the uncertainty in the outcome y given new observations \mathbf{x} . Conditional densities are also central to Bayesian inference. A key component of Bayesian parameter inference is the posterior distribution $f(\theta|\mathbf{x})$, which

“close enough” to the true density. Current goodness-of-fit diagnostics for conditional density models \hat{f} only test for a form of overall coherence between a data-averaged conditional (posterior) distribution and its marginal (prior) distribution, by computing so-called probability integral transform (PIT) values [Cook et al., 2006, Freeman et al., 2017, Talts et al., 2018, D’Isanto and Polsterer, 2018]. Although these diagnostic methods provide valuable information to practitioners, they were originally developed for assessing unconditional density models [Gan and Koehler, 1990]; as such, they are unable to detect some clearly misspecified conditional models. Indeed, PIT diagnostics are insensitive to covariate transformations (Theorem 1). As an example, models trained on only a subset of the features can pass these checks (see Section 4).

In this paper, we present a new validation framework specifically developed for assessing the quality of fit of a conditional density model or Bayesian inference algorithm. To enrich our vocabulary for desired properties of conditional density estimators (CDEs), we begin by defining global and local consistency (see Definitions 1 and 3, respectively). We then propose a validation approach that efficiently estimates the coverage of a conditional density model $\hat{f}(\cdot|\mathbf{x})$ at every location \mathbf{x} in the feature space. Our proposed machinery has three main components:

- **[GCT - Global Coverage Test]** A statistical hypothesis test that is able to distinguish *any* misspecified density model from the true conditional density. (This is a test of global consistency.)
- **[LCT - Local Coverage Test]** A statistical hypothesis test that is able to tell *where* in the feature space the model needs to be improved. (This is a test of local consistency.)
- **[ALP - Amortized Local P-P plots]** A visualization tool that quickly provides interpretable graphical summaries of the fitted model by showing *how* it deviates from the true density at any location in feature space (see Figure 1 for examples).

Our proposed diagnostics are easy to compute, and can quickly identify, locate, and interpret the nature of (statistically significant) discrepancies over the entire feature space. At the heart of our approach is the realization that the local coverage of a CDE model is itself a conditional probability (see Equation 5) that often varies smoothly with \mathbf{x} . Hence, we can estimate the local coverage at any given \mathbf{x} by leveraging a suitable regression method using sample points in a neighborhood of \mathbf{x} . Thanks to the impressive arsenal of existing regression methods, we can adapt to different types of potentially high-dimensional data to obtain computationally and statistically efficient validation. Finally, because we specifically evaluate local coverage (rather than other types of discrepancies), the practitioner can, when the LCT flags statistically significant local discrepancies, “zoom in” on

those locations and identify common modes of failure in the fitted conditional density (see Figures 4 and 5 for examples).

This paper is organized as follows: in Section 2, we define properties that goodness-of-fit tests would ideally have, and show how existing diagnostics may not satisfy them. In Section 3, we introduce our new diagnostic framework with GCT, LCT, and ALP. In Section 4, we show that our framework can identify and diagnose omitted variable bias of CDE in a prediction setting. In Section 5, we consider a realistic application of validation of Bayesian inference algorithms fit to high-dimensional simulated galaxy images.

2 EXISTING DIAGNOSTICS ARE INSENSITIVE TO COVARIATE TRANSFORMATIONS

Notation. Let $\mathcal{D} = \{(\mathbf{X}_1, Y_1), \dots, (\mathbf{X}_n, Y_n)\}$ denote an i.i.d. sample from $F_{\mathbf{X}, Y}$, the joint distribution of (\mathbf{X}, Y) for a random variable $Y \in \mathcal{Y} \subset \mathbb{R}$ (in Section 3.3, Y is multivariate), and a random vector $\mathbf{X} \in \mathcal{X} \subset \mathbb{R}^d$. In a prediction setting, \mathcal{D} represents a hold-out set not used to train \hat{f} . In a Bayesian setting, Y represents the parameter of interest (sometimes also denoted with θ), and each element of \mathcal{D} is obtained by first drawing Y_i from the prior distribution, and then drawing \mathbf{X}_i from the statistical model of $\mathbf{X}|Y_i$.

Our goal is to check whether the conditional density model $\hat{f}(y|\mathbf{x})$ is a good estimate of the true density $f(y|\mathbf{x})$. Ideally, such a test should be able to distinguish any model $\hat{f}(y|\mathbf{x})$ from the true density $f(y|\mathbf{x})$, as well as locate discrepancies in the feature space \mathcal{X} . More precisely, a test should be able to identify what we in this section define as global and local consistency.

Definition 1 (Global Consistency). *An estimate $\hat{f}(y|\mathbf{x})$ is globally consistent with the density $f(y|\mathbf{x})$ if the following null hypothesis holds:*

$$H_0 : \hat{f}(y|\mathbf{x}) = f(y|\mathbf{x}) \text{ for almost every } \mathbf{x} \in \mathcal{X} \text{ and } y \in \mathcal{Y}. \quad (1)$$

Existing diagnostics typically calibrate density models by computing PIT values on independent data, which were not used to estimate $\hat{f}(y|\mathbf{x})$:

Definition 2 (PIT). *Fix $\mathbf{x} \in \mathcal{X}$ and $y \in \mathcal{Y}$. The probability integral transform of y at \mathbf{x} , as modeled by the conditional density estimate $\hat{f}(y|\mathbf{x})$, is*

$$PIT(y; \mathbf{x}) = \int_{-\infty}^y \hat{f}(y'|\mathbf{x}) dy'. \quad (2)$$

See Figure 2, top panel for an illustration of this calculation.

Remark 1. *For implicit models of $\hat{f}(y|\mathbf{x})$ (that is, generative models that via e.g. MCMC can sample from, but not directly evaluate $\hat{f}(y|\mathbf{x})$), we can approximate the PIT values by forward-simulating data: For fixed $\mathbf{x} \in \mathcal{X}$ and $y \in \mathcal{Y}$,*

draw $Y_1, \dots, Y_L \sim \widehat{f}(\cdot|\mathbf{x})$. Then, approximate PIT(y ; \mathbf{x}) via the cumulative sum $\frac{1}{L} \sum_{i=1}^L \mathbb{I}(y_i \leq y)$.

If the conditional density model $\widehat{f}(y|\mathbf{x})$ is globally consistent, then the PIT values are uniformly distributed. More precisely, if H_0 (Equation 1) is true, then the random variables $\text{PIT}(Y_1; \mathbf{X}_1), \dots, \text{PIT}(Y_n; \mathbf{X}_n) \stackrel{i.i.d.}{\sim} \text{Unif}(0, 1)$. This result is often used to test goodness-of-fit of conditional density models in practice [Cook et al., 2006, Bordoloi et al., 2010, Tanaka et al., 2018].

Our first point is that unfortunately, such random variables can be uniformly distributed even if global consistency does not hold. This is shown in the following theorem.

Theorem 1 (Insensitivity to covariate transformations). *Suppose there exists a function $g : \mathcal{X} \rightarrow \mathcal{Y}$ that satisfies*

$$\widehat{f}(y|\mathbf{x}) = f(y|g(\mathbf{x})). \quad (3)$$

Let $(\mathbf{X}, Y) \sim F_{\mathbf{X}, Y}$. Then $\text{PIT}(Y; \mathbf{X}) \sim \text{Unif}(0, 1)$.

Many models naturally lead to estimates that could satisfy the condition in Equation 3, even without being globally consistent. In fact, clearly misspecified models \widehat{f} can yield uniform PIT values and “pass” an associated goodness-of-fit test regardless of the sample size. For example: if $\widehat{f}(y|\mathbf{x})$ is based on a linear model, then the estimate $\widehat{f}(y|\mathbf{x})$ will by construction depend on \mathbf{x} only through $g(\mathbf{x}) := \beta^T \mathbf{x}$ for some $\beta \in \mathbb{R}^d$. As a result, we could have $\widehat{f}(y|\mathbf{x}) = f(y|g(\mathbf{x}))$ even when $\widehat{f}(y|\mathbf{x})$ is potentially very different from $f(y|\mathbf{x})$. As another example, a conditional density estimator that performs variable selection [Shiga et al., 2015, Izbicki et al., 2017b, Dalmaso et al., 2020] could satisfy $\widehat{f}(y|\mathbf{x}) = f(y|g(\mathbf{x}))$ for $g(\mathbf{x}) := (\mathbf{x})_S$, where $S \subset \{1, \dots, d\}$ is a subset of the covariates. A test of the overall uniformity of PIT values is no guarantee that we are correctly modeling the relationship between y and the predictors \mathbf{x} ; see Figure 3 for an illustration.

Our second point is that current diagnostics also do not pinpoint the locations in feature space \mathcal{X} where the estimates of f should be improved. Hence, in addition to global consistency, we need diagnostics that test the following property:

Definition 3 (Local Consistency). *Fix $\mathbf{x} \in \mathcal{X}$. An estimate $\widehat{f}(y|\mathbf{x})$ is locally consistent with the density $f(y|\mathbf{x})$ at fixed \mathbf{x} if the following null hypothesis holds*

$$H_0(\mathbf{x}) : \widehat{f}(y|\mathbf{x}) = f(y|\mathbf{x}) \text{ for every } y \in \mathcal{Y}. \quad (4)$$

In the next section, we introduce new diagnostics that are able to test whether a conditional density model \widehat{f} is both globally and locally consistent with the underlying conditional distribution f of the data. Our diagnostics are still based on PIT, and hence retain the properties (e.g., interpretability, ability to provide graphical summaries, and so on) that have made PIT a popular choice in model validation.

3 NEW DIAGNOSTICS TEST LOCAL AND GLOBAL CONSISTENCY

Our new diagnostics rely on the following key result:

Theorem 2 (Local Consistency and Pointwise Uniformity). *For any $\mathbf{x} \in \mathcal{X}$, the local null hypothesis $H_0(\mathbf{x}) : \widehat{f}(\cdot|\mathbf{x}) = f(\cdot|\mathbf{x})$ holds if, and only if, the distribution of $\text{PIT}(Y; \mathbf{x})$ given \mathbf{x} is uniform over $(0, 1)$.*

Theorem 2 implies that if we had a sample of Y ’s at the fixed location \mathbf{x} , we could test the local consistency (Definition 3) of \widehat{f} by determining whether the sample’s PIT values come from a uniform distribution. In addition, for global consistency we need local consistency at every $\mathbf{x} \in \mathcal{X}$. Clearly, such a testing procedure would not be practical: typically, we have data of the form $(\mathbf{X}_1, Y_1), \dots, (\mathbf{X}_n, Y_n)$ with at most one observation at any given $\mathbf{x} \in \mathcal{X}$.

Our solution is to instead address this problem as a regression: for fixed $\alpha \in (0, 1)$, we consider the cumulative distribution function (CDF) of PIT at \mathbf{x} ,

$$r_\alpha(\mathbf{x}) := \mathbb{P}(\text{PIT}(Y; \mathbf{x}) < \alpha|\mathbf{x}), \quad (5)$$

which interestingly is the regression of the random variable $Z^\alpha := \mathbb{I}(\text{PIT}(Y; \mathbf{X}) < \alpha)$ on \mathbf{X} .

From Theorem 2, it follows that the estimated density is locally consistent at \mathbf{x} if and only if $r_\alpha(\mathbf{x}) = \alpha$ for every α :

Corollary 1. *Fix $\mathbf{x} \in \mathcal{X}$. Then $r_\alpha(\mathbf{x}) = \alpha$ for every $\alpha \in (0, 1)$ if, and only if, $\widehat{f}(y|\mathbf{x}) = f(y|\mathbf{x})$ for every $y \in \mathcal{Y}$.*

Our new diagnostics are able to test for both local and global consistency. They rely on the simple idea of estimating $r_\alpha(\mathbf{x})$ and then evaluating how much it deviates from α (see Section 3.1). Note that

$$\text{PIT}(Y; \mathbf{x}) < \alpha \iff Y \in (-\infty, \widehat{q}_\alpha(\mathbf{x}))$$

where $\widehat{q}_\alpha(\mathbf{x})$ is the α -quantile of \widehat{f} . That is, $r_\alpha(\mathbf{x})$ evaluates the local level- α coverage of \widehat{f} at \mathbf{x} . In Section 3.2, we explore the connection between test statistics and coverage, for interpretable descriptions of how conditional density models \widehat{f} may fail to approximate the true conditional density f .

3.1 LOCAL AND GLOBAL COVERAGE TESTS

Our procedure for testing local and global consistency is very simple and can be adapted to different types of data. For an i.i.d. test sample $(\mathbf{X}_1, Y_1), \dots, (\mathbf{X}_n, Y_n)$ from $F_{\mathbf{X}, Y}$ (which was not used to construct \widehat{f}), we compute $Z_i^\alpha := \mathbb{I}(\text{PIT}(Y_i; \mathbf{X}_i) < \alpha)$. To estimate the coverage $r_\alpha(\mathbf{x})$ (Equation 5) for any $\mathbf{x} \in \mathcal{X}$, we then simply regress Z on \mathbf{X} using the transformed data $(\mathbf{X}_1, Z_1), \dots, (\mathbf{X}_n, Z_n)$. Numerous classes of regression estimators can be used, from kernel smoothers to random forests to neural networks.

To test local consistency (Definition 3), we introduce the *Local Coverage Test* (LCT) with the test statistic

$$T(\mathbf{x}) := \frac{1}{|G|} \sum_{\alpha \in G} (\hat{r}_\alpha(\mathbf{x}) - \alpha)^2,$$

where \hat{r}_α denotes the regression estimator and G is a grid of α values. Large values of $T(\mathbf{x})$ indicate a large discrepancy between \hat{f} and f at \mathbf{x} in terms of coverage, and Corollary 1 links coverage to consistency. To decide on the correct cutoff for rejecting $H_0(\mathbf{x})$, we use a Monte Carlo technique that simulates $T(\mathbf{x})$ under H_0 . Algorithm 1 details our procedure.

Similarly, we can also test global consistency (Definition 1) with a Monte Carlo strategy. We introduce the *Global Coverage Test* (GCT) based on the following test statistic:

$$S := \frac{1}{n} \sum_{i=1}^n T(\mathbf{X}_i).$$

We recommend performing the global test first and, if the global null is rejected, investigating further with local tests.

Algorithm 1 P-values for Local Coverage Test

Require: conditional density model \hat{f} ; test data $\{\mathbf{X}_i, Y_i\}_{i=1}^n$; test point $\mathbf{x} \in \mathcal{X}$; regression estimator \hat{r} ; number of null training samples B

Ensure: estimated p-value $\hat{p}(\mathbf{x})$ for any $\mathbf{x} \in \mathcal{X}$

```

1: // Compute test statistic at  $\mathbf{x}$ :
2: Compute values  $\text{PIT}(Y_1; \mathbf{X}_1), \dots, \text{PIT}(Y_n; \mathbf{X}_n)$ 
3:  $G \leftarrow$  grid of  $\alpha$  values in  $(0, 1)$ .
4: for  $\alpha$  in  $G$  do
5:   Compute indicators  $Z_1^\alpha, \dots, Z_n^\alpha$ 
6:   Train regression method  $\hat{r}_\alpha$  on  $\{\mathbf{X}_i, Z_i^\alpha\}_{i=1}^n$ 
7: end for
8: Compute test statistic  $T(\mathbf{x})$ 
9: // Recompute test statistic under null distribution:
10: for  $b$  in  $1, \dots, B$  do
11:   Draw  $U_1^{(b)}, \dots, U_n^{(b)} \sim \text{Unif}[0, 1]$ .
12:   for  $\alpha$  in  $G$  do
13:     Compute indicators  $\{Z_{\alpha,i}^{(b)} = \mathbb{I}(U_i^{(b)} < \alpha)\}_{i=1}^n$ 
14:     Train regression method  $\hat{r}_\alpha^{(b)}$  on  $\{\mathbf{X}_i, Z_{\alpha,i}^{(b)}\}_{i=1}^n$ 
15:   end for
16:   Compute  $T^{(b)}(\mathbf{x}) := \frac{1}{|G|} \sum_{\alpha \in G} (\hat{r}_\alpha^{(b)}(\mathbf{x}) - \alpha)^2$ 
17: end for
18: return  $\hat{p}(\mathbf{x}) := \frac{1}{B} \sum_{b=1}^B \mathbb{I}(T(\mathbf{x}) < T^{(b)}(\mathbf{x}))$ 

```

3.2 AMORTIZED LOCAL P-P PLOTS

Our diagnostic framework does not just give us the ability to identify deviations from local consistency in different parts of the feature space \mathcal{X} . It also provides us with insight into the nature of such deviations at any given location \mathbf{x} .

For unconditional density models, data scientists have long favored using P-P plots (which plot two cumulative distribution functions against each other) to assess how closely a density model agrees with actual observed data. What makes our work unique is that we are able to construct ‘‘amortized local P-P plots’’ (ALPs) with similar interpretations to assess *conditional* density models over the entire feature space.

Figure 1 illustrates how a local P-P plot of $\hat{r}_\alpha(\mathbf{x})$ against α (that is, the estimated CDF against the true CDF at \mathbf{x}) can identify different types of deviations in a conditional density model. For example, positive or negative bias in the estimated density \hat{f} relative to f leads to P-P plot values that are too high or too low, respectively. We can also easily identify overdispersion or underdispersion of \hat{f} from an ‘‘S’’-shaped P-P plot.

Of particular note is that our local P-P plots are ‘‘amortized’’, in the sense that computationally expensive steps do not have to be repeated with e.g Monte Carlo sampling at each \mathbf{x} of interest. Both the consistency tests in Section 3.1 and the local P-P plots only require initially training \hat{r}_α on the observed data; the regression estimator can then be used to compute $\hat{r}_\alpha(\mathbf{x}_{val})$ at any new evaluation point \mathbf{x}_{val} . Because of the flexibility in the choice of regression method, our construction also potentially scales to high-dimensional or different types of data \mathbf{x} . Algorithm 2 details the construction of ALPs, including how to compute confidence bands by a Monte Carlo algorithm.

Algorithm 2 Confidence bands for local P-P plot

Require: test data $\{\mathbf{X}_i\}_{i=1}^n$; test point $\mathbf{x} \in \mathcal{X}$; regression estimator \hat{r} ; number of null training samples B ; confidence level η

Ensure: estimated upper and lower confidence bands $U(\mathbf{x}), L(\mathbf{x})$ at level $1 - \eta$ for any $\mathbf{x} \in \mathcal{X}$

```

1: // Recompute regression under null distribution:
2:  $G \leftarrow$  grid of  $\alpha$  values in  $(0, 1)$ .
3: for  $b$  in  $1, \dots, B$  do
4:   Draw  $U_1^{(b)}, \dots, U_n^{(b)} \sim \text{Unif}[0, 1]$ .
5:   for  $\alpha$  in  $G$  do
6:     Compute indicators  $\{Z_{\alpha,i}^{(b)} = \mathbb{I}(U_i^{(b)} < \alpha)\}_{i=1}^n$ 
7:     Train regression method  $\hat{r}_\alpha^{(b)}$  on  $\{\mathbf{X}_i, Z_{\alpha,i}^{(b)}\}_{i=1}^n$ 
8:   end for
9:   Compute  $\hat{r}_\alpha^{(b)}(\mathbf{x})$ 
10: end for
11: // Compute  $(1 - \eta)$  confidence bands for  $\hat{r}_\alpha(\mathbf{x})$ :
12:  $U(\mathbf{x}), L(\mathbf{x}) \leftarrow \emptyset$ 
13: for  $\alpha$  in  $G$  do
14:    $U(\mathbf{x}) \leftarrow U(\mathbf{x}) \cup (1 - \frac{\eta}{2})$ -quantile of  $\{\hat{r}_\alpha^{(b)}(\mathbf{x})\}_{b=1}^B$ 
15:    $L(\mathbf{x}) \leftarrow L(\mathbf{x}) \cup \frac{\eta}{2}$ -quantile of  $\{\hat{r}_\alpha^{(b)}(\mathbf{x})\}_{b=1}^B$ 
16: end for
17: return  $U(\mathbf{x}), L(\mathbf{x})$ 

```

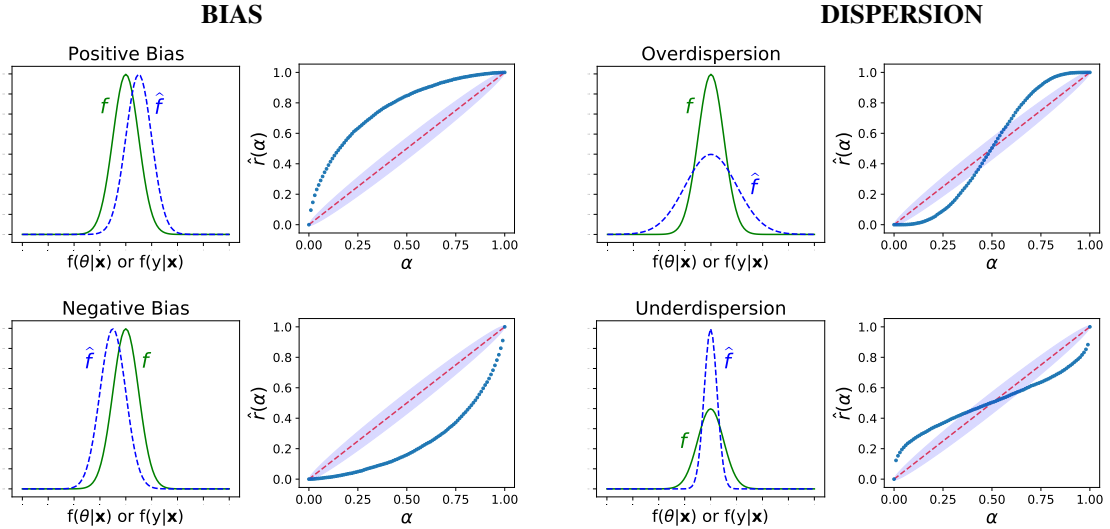


Figure 1: P-P plots are commonly used to assess how well a density model fits actual data. Such plots display, in a clear and interpretable way, effects like bias (left panel) and dispersion (right panel) in an estimated distribution \hat{f} vis-a-vis the true data-generating distribution f . Our framework yields a computationally efficient way to construct “amortized local P-P plots” for validating posterior distributions $\hat{f}(\theta|\mathbf{x})$ and conditional density models $\hat{f}(y|\mathbf{x})$, at any location \mathbf{x} of the feature space \mathcal{X} , thus providing insight into how such estimates can be improved. See text for details and Sections 4 and 5 for examples.

3.3 HANDLING MULTIVARIATE RESPONSES

If the response \mathbf{Y} is multivariate, then the random variable $F_{\mathbf{Y}|\mathbf{X}}(\mathbf{Y}|\mathbf{X})$ is not uniformly distributed [Genest and Rivest, 2001], so PIT values cannot be trivially generalized to higher dimensions. One way to overcome this is to evaluate the PIT statistic of univariate projections of \mathbf{Y} , as done by Talts et al. [2018] for Bayesian consistency checks and Mucesh et al. [2020] for the prediction setting. That is, the PIT values can be computed using the estimate $\hat{f}(h(\mathbf{Y})|\mathbf{x})$ induced by $\hat{f}(\mathbf{Y}|\mathbf{x})$ for some chosen $h: \mathbb{R}^p \rightarrow \mathbb{R}$. Different projections can be used depending on the context. For instance, in Bayesian applications, posterior distributions are often used to compute credible regions for univariate projections of the parameters θ . Thus, it is natural to evaluate PIT values of $h(\theta) = \theta_i$ for each parameter of interest. Another useful projection is copPIT [Ziegel et al., 2014], which creates a uni-dimensional projection that has information about the joint distribution of \mathbf{Y} . Even though our diagnostic techniques applied to these projections are not enough to consistently assess the fit to $f(\mathbf{Y}|\mathbf{x})$, they do consistently evaluate the fit to $f(h(\mathbf{Y})|\mathbf{x})$, which is often good enough in practice.

An alternative approach to assessing \hat{f} is through highest predictive density values (HPD values; Harrison et al. 2015, Dalmaso et al. 2020), which are defined by

$$\text{HPD}(\mathbf{y}; \mathbf{x}) = \int_{\mathbf{y}': \hat{f}(\mathbf{y}'|\mathbf{x}) \geq \hat{f}(\mathbf{y}|\mathbf{x})} \hat{f}(\mathbf{y}'|\mathbf{x}) d\mathbf{y}$$

(see Figure 2, bottom, for an illustration). $\text{HPD}(\mathbf{y}; \mathbf{x})$ is a measure of how plausible \mathbf{y} is according to $\hat{f}(\mathbf{y}|\mathbf{x})$ (in the

Bayesian context, this is the complement of the e-value [de Bragança Pereira and Stern, 1999]; small values indicate high plausibility). As with PIT values, HPD values are uniform under the global null hypothesis [Dalmaso et al., 2020]. However, standard goodness-of-fit tests based on HPD values share the same problem as those based on PIT: they are insensitive to covariate transformations (see Theorem 4, Supp. Mat. A). Fortunately, HPD values are uniform under the local consistency hypothesis:

Theorem 3. *For any $\mathbf{x} \in \mathcal{X}$, if the local null hypothesis $H_0(\mathbf{x}) : \hat{f}(\cdot|\mathbf{x}) = f(\cdot|\mathbf{x})$ holds, then the distribution of $\text{HPD}(Y; \mathbf{x})$ given \mathbf{x} is uniform over $(0, 1)$.*

It follows that the same techniques developed in Sections 3.1 and 3.2 can be used with HPD values to test the global and local consistency hypotheses for multivariate responses, as well as to construct amortized local P-P plots. This statistic is especially appealing if one wishes to construct predictive regions with \hat{f} , as HPD values are intrinsically related to highest predictive density sets [Hyndman, 1996]. HPD sets are region estimates of \mathbf{y} that contain all \mathbf{y} 's for which $\hat{f}(\mathbf{y}|\mathbf{x})$ is larger than a certain threshold (in the Bayesian case, these are the high posterior credible regions). More precisely, if $\text{HPD}_{1-\alpha}(\mathbf{x})$ is the $(1 - \alpha)$ -level HPD set for \mathbf{y} , then

$$\text{HPD}(\mathbf{y}; \mathbf{x}) > \alpha \iff Y \in \text{HPD}_{1-\alpha}(\mathbf{x}).$$

Thus, by testing local consistency of \hat{f} via HPD values, we are automatically assessing the coverage of HPD sets. It should be noted, however, that even if the HPD values are uniform (conditional on \mathbf{x}), it may be the case that $\hat{f} \neq f$.

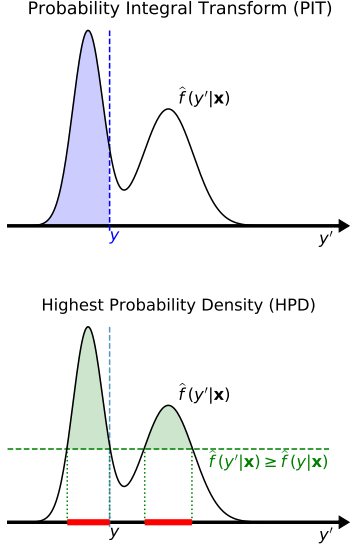


Figure 2: Schematic diagram of the construction of PIT (top panel, shaded blue region) and HPD values (bottom panel, shaded green region) for an estimated density \hat{f} evaluated at (y, \mathbf{x}) . The highlighted intervals in the bottom panel correspond to the highest density regions (HDR) of $y|\mathbf{x}$.

4 EXAMPLE 1: OMITTED VARIABLE BIAS IN CDE MODELS

Our first example shows how our tools are useful for diagnosing omitted but clearly relevant variables in a prediction setting. Inspired by Section 2.2.2 of Shalizi [2013], we generate two covariates according to $\mathbf{X} = (X_1, X_2) \sim N(0, \Sigma) \in \mathbb{R}^2$, with $\Sigma_{1,1} = \Sigma_{2,2} = 1$ and $\Sigma_{1,2} = 0.8$, and take the response to be $Y|\mathbf{X} \sim N(X_1 + X_2, 1)$. In order to mimic the variable selection procedure common in many high-dimensional inference methods, we fit two conditional density models: \hat{f}_1 , trained only on X_1 , and \hat{f}_2 , trained on \mathbf{X} . Both models are here fitted using a nearest-neighbor kernel CDE [Dalmasso et al., 2020] with hyperparameters chosen by data-splitting. We use 10000 training and 5000 validation points, and a test sample of 200 points to assess the models.

This is a toy example where omitting one of the two variables might lead to unwanted bias when predicting the outcome Y for new inputs \mathbf{X} . As an indication of this bias, we have included a heat map (see panel (d) of Figure 4) of the difference in the true (unknown) conditional means, $\mathbb{E}[Y|x_1] - \mathbb{E}[Y|x_1, x_2]$ as a function of x_1 and x_2 . (In this example, the omitted variable bias is approximately the same as the difference in the averages of the predictions of Y when using the model \hat{f}_1 versus the model \hat{f}_2 at any given $\mathbf{x} \in \mathcal{X}$; see Figure 4 panels (c) and (d)). Despite the fact that there is a clear relationship between Y and X_2 , both \hat{f}_1 (which omits X_2) and \hat{f}_2 pass existing goodness-of-fit tests based on PIT (Figure 3). This result can be explained by Theorem

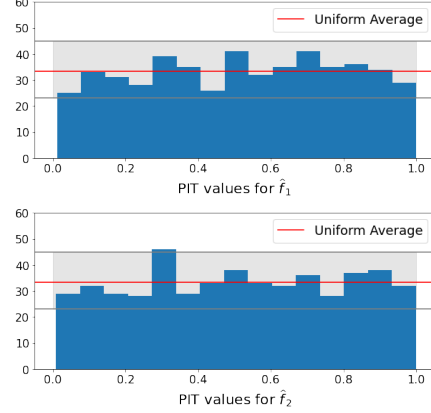


Figure 3: Standard diagnostics for Example 1 showing histograms of PIT values computed on 200 test points (with 95% confidence bands for a $\text{Unif}[0,1]$ distribution). *Top*: Results for \hat{f}_1 , which has only been fit to the first of two covariates. *Bottom*: Results for \hat{f}_2 , which has been fit to both covariates. The top panel shows that standard PIT diagnostics cannot tell that \hat{f}_1 is a poor approximation to f . GCT, on the other hand, detects that \hat{f}_1 is misspecified ($p=0.004$), while not rejecting the global null for \hat{f}_2 ($p=0.894$).

1: because PIT is insensitive to covariate transformations and $\hat{f}_1(y|\mathbf{x}) \approx \hat{f}(y|x_1)$, PIT values are uniformly distributed, even though \hat{f}_1 omits a key variable. The GCT, however, detects that \hat{f}_1 is misspecified ($p = 0.004$), while the global null (Equation 1) is not rejected for \hat{f}_2 ($p = 0.894$).

The next question a practitioner might ask is: “What exactly is wrong with the fit?”. LCTs and local P-P plots can provide insight here by pinpointing the locations of discrepancies, as well as by describing the modes of failure. Panel (a) of Figure 4 shows p-values from local coverage tests for \hat{f}_1 across the entire feature space of \mathbf{X} . The patterns in these p-values are largely explained by panel (d), which shows the difference between the conditional means of Y given x_1 and given x_1, x_2 . The detected level of discrepancy between the estimate \hat{f}_1 and the true underlying conditional density f at a point \mathbf{x} directly relates to the omitted variable bias $\mathbb{E}[Y|x_1] - \mathbb{E}[Y|x_1, x_2] = 0.8x_1 - x_2$: the LCT p-values close to the line $x_2 = 0.8x_1$ are large (indicating no statistically significant deviations from the true model), and p-values get smaller as we move away from this line.

As an illustration of how one can depict and interpret distributional deviations at specific points of interest \mathbf{x} , panel (b) of Figure 4 zooms in on a few different locations, with local P-P plots that show how \hat{f}_1 could potentially be improved. At the blue point, \hat{f}_1 underestimates the true density: we reject the local null (Equation 4) at level $\alpha = 0.05$, and the P-P plot indicates negative bias. Conversely, at the red point, \hat{f}_1 overestimates the true density; we reject the local null, and the P-P plot indicates positive bias. At the purple point, \hat{f}_1 is close to f , so the local null hypothesis is not rejected.

Finally, the right panel of Figure 6 (in Supp. Mat. B) shows

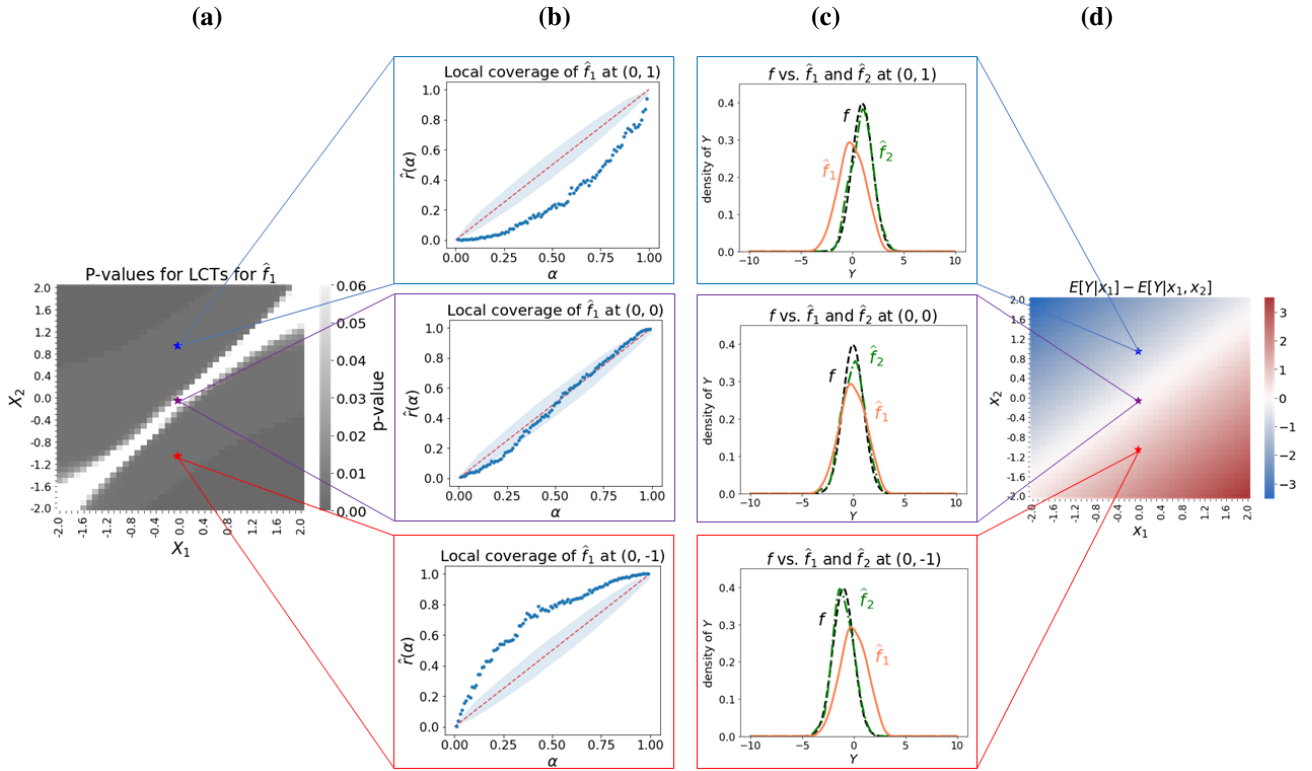


Figure 4: New diagnostics for Example 1. (a) P-values for LCTs for \hat{f}_1 indicate a poor fit across most of the feature space. (b) Amortized local P-P plots at selected points show the density \hat{f}_1 as negatively biased (blue), well estimated at significance level $\alpha = 0.05$ with barely perceived overdispersion (purple), and positively biased (red). (Gray regions represent 95% confidence bands under the null.) (c) \hat{f}_1 and \hat{f}_2 vs. the true (unknown) conditional density f at the selected points. \hat{f}_1 is clearly negatively and positively biased at the blue and red points, respectively, while the model does not reject the local null at the purple point. \hat{f}_2 fits well at all three points. (d) The difference on average in the predictions of Y from $\hat{f}_1(\cdot|x)$ vs. the true distribution $f(\cdot|x)$ for fixed \mathbf{x} indeed corresponds to the “omitted variable bias” $\mathbb{E}[Y|x_1] - \mathbb{E}[Y|x_1, x_2]$. (Note: Panels (c) and (d) require knowledge of the true f , which would not be available to the practitioner.)

p-values from LCTs for the model \hat{f}_2 which was fit to both variables. Here \hat{f}_2 passes all tests, and local P-P plots at various points indicate a good fit.

This toy example is a simple illustration of the general phenomenon of potentially unwanted omitted variable bias, which can be difficult to detect without testing for local and global consistency of models. Our proposed diagnostics identify this issue and provide insight into how the omitted variable distorts the fitted model relative to the true conditional density, across the entire feature space.

5 EXAMPLE 2: POSTERIOR INFERENCE FOR SYNTHETIC GALAXY IMAGES

Our next example illustrates how our diagnostics can be used for simulator-based inference to test, for all possible values of image data $\mathbf{x} \in \mathbb{R}^{400}$, whether a Bayesian inference algorithm or approximation $\hat{f}(\theta|\mathbf{x})$ of the posterior fits the true posterior given by the model.

In this example, \mathbf{x} represents an image of an elliptical galaxy as observed by a telescope, and the parameter of interest is the galaxy’s rotation angle with respect to the x -axis. Our model for \mathbf{x} is implicitly given by `Galsim`, an open-source toolkit for simulating realistic images of astronomical objects that include observational effects such as pixelization and blurring due to the atmosphere and telescope [Rowe et al., 2015]. Besides θ , our model also contains another parameter, the axis ratio of the galaxy, λ , here defined as the ratio between the minor and major axes of the projection of the elliptical galaxy.

For illustration, we create a mixture of two populations of galaxies: one large population with $\lambda = 0.7$ (round galaxies), and a second smaller population with $\lambda = 0.1$ (elongated galaxies). We then simulate a sample of images as follows: first, we draw λ and θ from a prior distribution given by

$$\mathbb{P}(\lambda = 0.7) = 1 - \mathbb{P}(\lambda = 0.1) = 0.9$$

$$\theta \sim \text{Unif}(-\pi, \pi)$$

Then we sample 20×20 galaxy images \mathbf{X} according to the

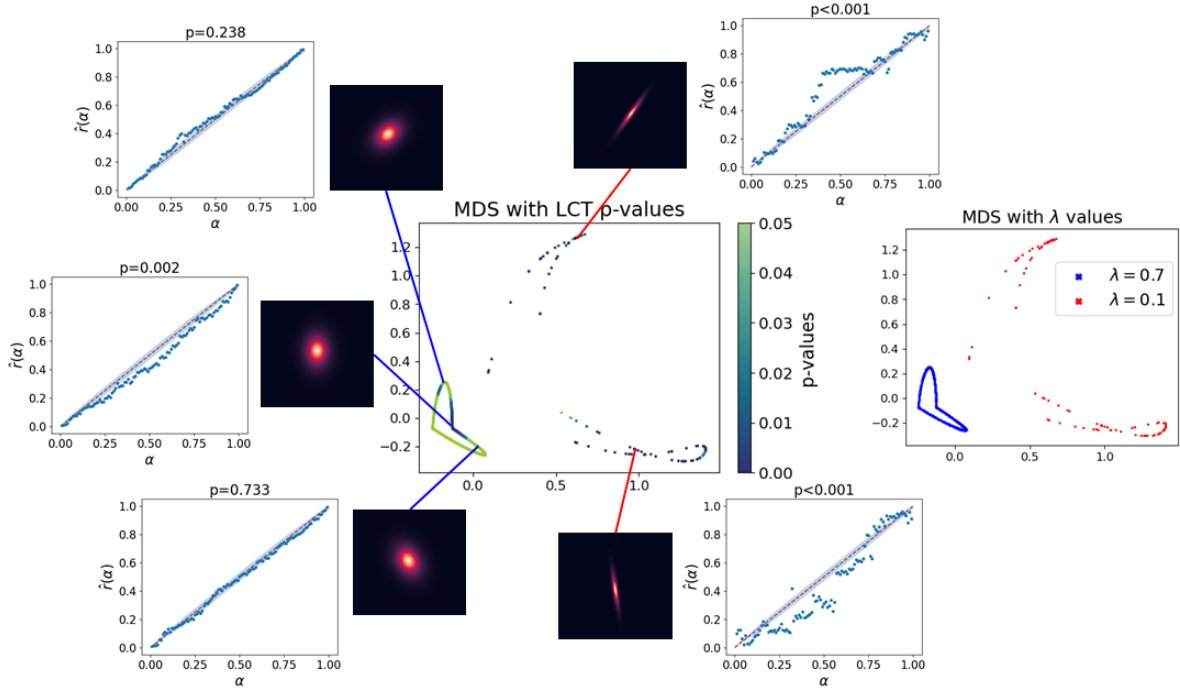


Figure 5: New diagnostics for simulation-based inference algorithm in Example 2. For visualization, we show the location of the test galaxy points in \mathbb{R}^{400} using multidimensional scaling (see center panel “MDS with LCT p-values”). P-values for LCTs indicate that the ConvMDN generally fits well for the dominant 90% population of round galaxies ($\lambda = 0.7$), while fitting poorly for the smaller 10% subpopulation of elongated galaxies ($\lambda = 0.1$). Local P-P plots show statistically significant deviations in the CDEs (gray regions are 95% confidence bands under the null) for the latter population, suggesting we need better approximations of the posterior for this group.

data model $\mathbf{X}|\lambda, \theta \sim \text{GalSim}(a, \lambda)$, where

$$a|\lambda = 0.7 \sim N(\theta, 0.05)$$

$$a|\lambda = 0.1 \sim \frac{1}{2}\text{Laplace}(\theta, 0.05) + \frac{1}{2}\text{Laplace}(\theta, 0.0005).$$

As an example of simulator-based inference, we fit a convolutional mixture density network (ConvMDN, D’Isanto and Polsterer [2018]) with 2 convolutional and 2 fully connected layers with ReLU activations [Glorot et al., 2011] to 7000 training images and 3000 validation images. (For training, we use the Adam optimizer [Kingma and Ba, 2014] with learning rate 10^{-3} , $\beta_1 = 0.9$, and $\beta_2 = 0.999$.) This gives us an estimate of the posterior distribution $f(\alpha|\mathbf{x})$.

According to the KL divergence loss computed on a separate test sample with 1000 images, the best fit of $f(\theta|\mathbf{x})$ is achieved by a ConvMDN model with $K = 7$ components (see Table 1 in Supp. Mat. C). However, loss functions only give us an overall measure of model discrepancy with test data. Our diagnostic framework, on the other hand, gives a fuller account of a candidate model’s goodness-of-fit as well as some guidance of potential improvements. Here, the ConvMDN model with the smallest KL loss fails the GCT ($p < 0.001$), so we turn to LCTs and P-P plots to understand why that is the case. Figure 5 plots the test galaxy images with multidimensional scaling using the first two

principal components. The LCTs show that the the posterior approximation with the smallest KL loss generally fits the density well for the main 90% population of rounder galaxies ($\lambda = 0.7$), but fails to model galaxies in the smaller 10% population of elongated galaxies ($\lambda = 0.1$). P-P plots at selected test points indicate severe bias in the posterior estimates for the $\lambda = 0.1$ population. Our localized P-P plots suggest that an effective way of obtaining a better approximation of the posterior is by improving the fit for the $\lambda = 0.1$ population (whether through obtaining more data in that region of the feature space, or by using a different model class, etc). For instance, CDE models that are not based on mixtures [Papamakarios et al., 2019] could be more effective.

Conclusion. Conditional density models are widely used for uncertainty quantification in prediction and Bayesian inference. In this work, we offer practical procedures (GCT, LCT, ALP) for identifying, localizing, and interpreting modes of failure for an approximation of the true conditional density. Our tools can be used in conjunction with loss functions, which are useful for performing model selection, but not good at evaluating whether a practitioner should keep looking for better models, or at providing information as to how a model could be improved. Finally, because LCT localizes hard-to-train areas of the feature space, our framework can provide guidance for active learning schemes.

References

- ABC–CDE: Toward approximate bayesian computation with complex high-dimensional data and limited simulations. *Journal of Computational and Graphical Statistics*, pages 1–20, 2019. doi: 10.1080/10618600.2018.1546594.
- R. Bordoloi, S. J. Lilly, and A. Amara. Photo-z performance for precision cosmology. *Monthly Notices of the Royal Astronomical Society*, 406(2):881–895, 08 2010. URL <https://doi.org/10.1111/j.1365-2966.2010.16765.x>.
- Steve Brooks, Andrew Gelman, Galin Jones, and Xiao-Li Meng. *Handbook of markov chain monte carlo*. CRC press, 2011.
- Yanzhi Chen and Michael U. Gutmann. Adaptive gaussian copula ABC. In Kamalika Chaudhuri and Masashi Sugiyama, editors, *Proceedings of Machine Learning Research*, volume 89 of *Proceedings of Machine Learning Research*, pages 1584–1592. PMLR, 16–18 Apr 2019. URL <http://proceedings.mlr.press/v89/chen19d.html>.
- Samantha R. Cook, Andrew Gelman, and Donald B. Rubin. Validation of software for bayesian models using posterior quantiles. *Journal of Computational and Graphical Statistics*, 15(3):675–692, 2006.
- Kyle Cranmer, Johann Brehmer, and Gilles Louppe. *Proceedings of the National Academy of Sciences*, 117(48):30055–30062, 2020.
- N. Dalmaso, T. Pospisil, A.B. Lee, R. Izbicki, P.E. Freeman, and A.I. Malz. Conditional density estimation tools in python and r with applications to photometric redshifts and likelihood-free cosmological inference. *Astronomy and Computing*, 30:100362, Jan 2020. ISSN 2213-1337. doi: 10.1016/j.ascom.2019.100362. URL <http://dx.doi.org/10.1016/j.ascom.2019.100362>.
- Carlos Alberto de Bragança Pereira and Julio Michael Stern. Evidence and credibility: full bayesian significance test for precise hypotheses. *Entropy*, 1(4):99–110, 1999.
- Antonio D’Isanto and Kai Lars Polsterer. Photometric redshift estimation via deep learning. generalized and pre-classification-less, image based, fully probabilistic redshifts. *Astronomy & Astrophysics*, 609:A111, 2018.
- Vincent Dutoit, Hugh Salimbeni, Marc Peter Deisenroth, and James Hensman. Gaussian process conditional density estimation. In *Advances in Neural Information Processing Systems 31*, Neural Information Processing Systems. Curran Associates, Inc., 2018.
- Peter Freeman, Rafael Izbicki, and Ann B. Lee. A unified framework for constructing, tuning and assessing photometric redshift density estimates in a selection bias setting. *Monthly Notices of the Royal Astronomical Society*, 468(4):4556–4565, 2017. doi: 10.1093/mnras/stx764.
- F. F. Gan and K. J. Koehler. Goodness-of-fit tests based on p-p probability plots. *Technometrics*, 32(3):289–303, 1990. doi: 10.1080/00401706.1990.10484682. URL <https://doi.org/10.1080/00401706.1990.10484682>.
- Christian Genest and Louis-Paul Rivest. On the multivariate probability integral transformation. *Statistics & probability letters*, 53(4):391–399, 2001.
- Xavier Glorot, Antoine Bordes, and Yoshua Bengio. Deep sparse rectifier neural networks. In Geoffrey Gordon, David Dunson, and Miroslav Dudík, editors, *Proceedings of the Fourteenth International Conference on Artificial Intelligence and Statistics*, volume 15 of *Proceedings of Machine Learning Research*, pages 315–323, Fort Lauderdale, FL, USA, 11–13 Apr 2011. JMLR Workshop and Conference Proceedings. URL <http://proceedings.mlr.press/v15/glorot11a.html>.
- David Greenberg, Marcel Nonnenmacher, and Jakob Macke. Automatic posterior transformation for likelihood-free inference. In Kamalika Chaudhuri and Ruslan Salakhutdinov, editors, *Proceedings of the 36th International Conference on Machine Learning*, volume 97 of *Proceedings of Machine Learning Research*, pages 2404–2414, Long Beach, California, USA, 09–15 Jun 2019. PMLR. URL <http://proceedings.mlr.press/v97/greenberg19a.html>.
- Diana Harrison, David Sutton, Pedro Carvalho, and Michael Hobson. Validation of Bayesian posterior distributions using a multidimensional Kolmogorov–Smirnov test. *Monthly Notices of the Royal Astronomical Society*, 451(3):2610–2624, 06 2015. ISSN 0035-8711. doi: 10.1093/mnras/stv1110. URL <https://doi.org/10.1093/mnras/stv1110>.
- Rob J Hyndman. Computing and graphing highest density regions. *The American Statistician*, 50(2):120–126, 1996.
- Rafael Izbicki, Ann B Lee, Peter E Freeman, et al. Photo-z estimation: An example of nonparametric conditional density estimation under selection bias. *Annals of Applied Statistics*, 11(2):698–724, 2017a.
- Rafael Izbicki, Ann B Lee, et al. Converting high-dimensional regression to high-dimensional conditional density estimation. *Electronic Journal of Statistics*, 11(2):2800–2831, 2017b.
- Diederik P. Kingma and Jimmy Ba. Adam: A method for stochastic optimization. *arXiv preprint arXiv:1412.6980*, 2014.

- Jan-Matthis Lueckmann, Pedro J. Gonçalves, Giacomo Bassetto, Kaan Öcal, Marcel Nonnenmacher, and Jakob H. Macke. Flexible statistical inference for mechanistic models of neural dynamics. In *Proceedings of the 31st International Conference on Neural Information Processing Systems*, NIPS'17, page 1289–1299, Red Hook, NY, USA, 2017. Curran Associates Inc. ISBN 9781510860964.
- Jean-Michel Marin, Louis Raynal, Pierre Pudlo, Mathieu Ribatet, and Christian Robert. ABC random forests for bayesian parameter inference. *Bioinformatics (Oxford, England)*, 35, 05 2016. doi: 10.1093/bioinformatics/bty867.
- S Mucesh, WG Hartley, A Palmese, O Lahav, L Whiteway, A Amon, K Bechtol, GM Bernstein, A Carnero Rosell, M Carrasco Kind, et al. A machine learning approach to galaxy properties: Joint redshift-stellar mass probability distributions with random forest. *arXiv preprint arXiv:2012.05928*, 2020.
- George Papamakarios and Iain Murray. Fast ϵ -free inference of simulation models with bayesian conditional density estimation. In D. Lee, M. Sugiyama, U. Luxburg, I. Guyon, and R. Garnett, editors, *Advances in Neural Information Processing Systems*, volume 29. Curran Associates, Inc., 2016. URL <https://proceedings.neurips.cc/paper/2016/file/6aca97005c68f1206823815f66102863-Paper.pdf>.
- George Papamakarios, Theo Pavlakou, and Iain Murray. Masked autoregressive flow for density estimation. *arXiv preprint arXiv:1705.07057*, 2017.
- George Papamakarios, David Sterratt, and Iain Murray. Sequential neural likelihood: Fast likelihood-free inference with autoregressive flows. In *22nd International Conference on Artificial Intelligence and Statistics*, Proceedings of Machine Learning Research, pages 837–848. PMLR, 2019.
- Jonas Rothfuss, Fabio Ferreira, Simon Walther, and Maxim Ulrich. Conditional density estimation with neural networks: Best practices and benchmarks, 2019.
- BTP Rowe, Mike Jarvis, Rachel Mandelbaum, Gary M Bernstein, James Bosch, Melanie Simet, Joshua E Meyers, Tomasz Kacprzak, Reiko Nakajima, Joe Zuntz, et al. Galsim: The modular galaxy image simulation toolkit. *Astronomy and Computing*, 10:121–150, 2015.
- Cosma Shalizi. *Advanced data analysis from an elementary point of view*. 2013.
- Motoki Shiga, Voot Tangkaratt, and Masashi Sugiyama. Direct conditional probability density estimation with sparse feature selection. *Machine Learning*, 100(2):161–182, 2015. doi: 10.1007/s10994-014-5472-x. URL <https://doi.org/10.1007/s10994-014-5472-x>.
- Scott A Sisson, Yanan Fan, and Mark Beaumont. *Handbook of Approximate Bayesian Computation*. Chapman and Hall/CRC, 2018.
- Kihyuk Sohn, Honglak Lee, and Xinchen Yan. Learning structured output representation using deep conditional generative models. In C. Cortes, N. Lawrence, D. Lee, M. Sugiyama, and R. Garnett, editors, *Advances in Neural Information Processing Systems*, volume 28. Curran Associates, Inc., 2015. URL <https://proceedings.neurips.cc/paper/2015/file/8d55a249e6baa5c06772297520da2051-Paper.pdf>.
- Sean Talts, Michael Betancourt, Daniel Simpson, Aki Vehtari, and Andrew Gelman. Validating bayesian inference algorithms with simulation-based calibration. *arXiv preprint arXiv:1804.06788*, 2018.
- Masayuki Tanaka, Jean Coupon, Bau-Ching Hsieh, Sogo Mineo, Atsushi J Nishizawa, Joshua Speagle, Hisanori Furusawa, Satoshi Miyazaki, and Hitoshi Murayama. Photometric redshifts for hyper supprime-cam subaru strategic program data release 1. *Publications of the Astronomical Society of Japan*, 70(SP1), 01 2018. URL <https://doi.org/10.1093/pasj/psx077>.
- Bengio Uria, Iain Murray, and Hugo Larochelle. A deep and tractable density estimator. In *Proceedings of the 31st International Conference on Machine Learning*, volume 32 of *Proceedings of Machine Learning Research*, Beijing, China, 09–15 Jun 2014. JMLR. URL <http://proceedings.mlr.press/v32/uria14.html>.
- Johanna F Ziegel, Tilmann Gneiting, et al. Copula calibration. *Electronic journal of statistics*, 8(2):2619–2638, 2014.

SUPPLEMENTARY MATERIALS

A: PROOFS

Proof of Theorem 1. Let $z = g(\mathbf{x})$. Notice that Equation 3 implies that $\widehat{F}(Y|\mathbf{x}) = F(Y|g(\mathbf{x})) = F(Y|z)$. Thus, if $(\mathbf{X}, Y) \sim F_{\mathbf{X}, Y}$ then, for every $0 \leq a \leq 1$,

$$\begin{aligned} \mathbb{P}(\text{PIT}(Y; \mathbf{X}) \leq a) &= \mathbb{P}(\widehat{F}(Y|\mathbf{X}) \leq a) \\ &= \int_{\mathcal{Z}} \mathbb{P}(\widehat{F}(Y|\mathbf{X}) \leq a|z) f(z) dz = \int_{\mathcal{Z}} \mathbb{P}(F(Y|Z) \leq a|z) f(z) dz \\ &= \int_{\mathcal{Z}} \mathbb{P}(F(Y|z) \leq a|z) f(z) dz = \int_{\mathcal{Z}} \mathbb{P}(Y \leq F^{-1}(a|z)|z) f(z) dz \\ &= \int_{\mathcal{Z}} F(F^{-1}(a|z)|z) f(z) dz = \int_{\mathcal{Z}} a f(z) dz = a. \end{aligned}$$

□

Proof of Theorem 2. Assume that $\widehat{f}(y|\mathbf{x}) = f(y|\mathbf{x})$. It follows that, for any $0 < \alpha < 1$,

$$\begin{aligned} \mathbb{P}(\text{PIT}(Y; \mathbf{X}) < 1 - \alpha|\mathbf{x}) &= \mathbb{P}(F_{Y|\mathbf{x}}(Y) \leq \alpha|\mathbf{x}) \\ &= \mathbb{P}(Y \leq F_{Y|\mathbf{x}}^{-1}(\alpha)|\mathbf{x}) \\ &= F_{Y|\mathbf{x}}(F_{Y|\mathbf{x}}^{-1}(\alpha)) \\ &= \alpha, \end{aligned}$$

which shows that the distribution of $\text{PIT}(Y; \mathbf{X})$, conditional on \mathbf{x} , is uniform. Now, assume that $\mathbb{P}(\text{PIT}(Y; \mathbf{X}) < 1 - \alpha|\mathbf{x}) = \alpha$ for every $0 < \alpha < 1$ and let $\widehat{F}_{Y|\mathbf{x}}(y) = \int_{-\infty}^y \widehat{f}(y'|\mathbf{x}) dy'$. Then

$$\begin{aligned} \alpha &= \mathbb{P}(\text{PIT}(Y; \mathbf{X}) < \alpha|\mathbf{x}) \\ &= \mathbb{P}(\widehat{F}_{Y|\mathbf{x}}(Y) \leq \alpha|\mathbf{x}) \\ &= \mathbb{P}(Y \leq \widehat{F}_{Y|\mathbf{x}}^{-1}(\alpha)|\mathbf{x}) \\ &= F_{Y|\mathbf{x}}(\widehat{F}_{Y|\mathbf{x}}^{-1}(\alpha)). \end{aligned}$$

It follows that $F_{Y|\mathbf{x}}(\widehat{F}_{Y|\mathbf{x}}^{-1}(\alpha)) = \alpha$, and thus

$$\widehat{F}_{Y|\mathbf{x}}^{-1}(\alpha) = F_{Y|\mathbf{x}}^{-1}(\alpha) \quad \forall \alpha \in (0, 1).$$

The conclusions follows from the fact that the CDF characterizes the distribution of a random variable. □

Proof of Corollary 1. Notice that $r_\alpha(\mathbf{x}) = \mathbb{E}[Z^\alpha|\mathbf{x}] = \mathbb{P}(\text{PIT}(Y; \mathbf{X}) < \alpha|\mathbf{x})$. It follows that $r_\alpha(\mathbf{x}) = \alpha$ for every $\alpha \in (0, 1)$ if, and only if, the distribution of $\text{PIT}(Y; \mathbf{X})$, conditional on \mathbf{X} , is uniform over $(0, 1)$. The conclusion follows from Theorem 2. □

Theorem 4 (HPD values are insensitive to covariate transformations). *Let $(\mathbf{X}, Y) \sim F_{\mathbf{X}, Y}$. If there exists a function $g : \mathcal{X} \rightarrow \mathcal{Z}$ such that $\widehat{f}(y|\mathbf{x}) = f(y|g(\mathbf{x}))$, then $\text{HPD}(Y; \mathbf{X}) \sim \text{Unif}(0, 1)$.*

Proof of Theorem 4. Under the assumption we can rewrite the HPD value as :

$$\begin{aligned} \text{HPD}(\mathbf{y}, \mathbf{x}) &= \int_{\mathbf{y}': f(\mathbf{y}'|g(\mathbf{x})) > f(\mathbf{y}|g(\mathbf{x}))} f(\mathbf{y}'|g(\mathbf{x})) dy' \\ &= \int_{\mathbf{y}': f(\mathbf{y}'|z) > f(\mathbf{y}|z)} f(\mathbf{y}'|z) dy' = \text{HPD}(\mathbf{y}, z), \end{aligned}$$

with $g(\mathbf{x}) = z$. Following the proof structure by Harrison et al. [2015] closely, we define the random variable $\xi_{z, \mathbf{y}} = \text{HPD}(z, \mathbf{y})$, equipped with the probability density function $h : (\mathcal{Z} \times \mathcal{Y}) \rightarrow \mathbb{R}$. Dropping the subscripts for simplicity, let $\xi^* = \text{HPD}(z^*, \mathbf{y}^*)$ the HPD value of a specific pair (z^*, \mathbf{y}^*) ; ξ^* is the probability mass of f above the level set $f(\mathbf{y}^*|z^*) = g(\mathbf{x}^*)$. Without loss of generality, if we show that $h(\xi^*) = 1$ we can conclude that $\xi(y, z)$ is uniformly distributed $U[0, 1]$. Using the fundamental theorem of calculus we can write:

$$\begin{aligned} h(\xi^*) &= \frac{\partial}{\partial \xi^*} \int_{-\infty}^{\xi^*} g(\varepsilon) d\varepsilon \\ &= \frac{\partial}{\partial \xi^*} \int_{-\infty}^{\xi^*} \int_{\mathcal{Z} \times \mathcal{Y}} \delta(\xi(y, z) - \varepsilon) dF(z, y) d\varepsilon \\ &= \frac{\partial}{\partial \xi^*} \int_{\mathcal{Z} \times \mathcal{Y}} \Phi(\xi(y, z) - \xi^*) dF(z, y) \\ &= \frac{\partial}{\partial \xi^*} \int_{\mathcal{Z}} \left[\int_{\mathcal{Y}} \Phi(\xi(y, z) - \xi^*) f(y|z) dy \right] f(z) dz \\ &= \frac{\partial}{\partial \xi^*} \int_{\mathcal{Z}} \xi^* f(z) dz = \frac{\partial}{\partial \xi^*} \xi^* = 1 \end{aligned}$$

where Φ is the Heavyside function, which is 1 when the argument is positive and 0 otherwise. □

Proof of Theorem 3. Under the null hypothesis $H_0(\mathbf{x})$ for any $\mathbf{x} \in \mathcal{X}$ we have that:

$$\text{HPD}(\mathbf{y}; \mathbf{x}) = \int_{\mathbf{y}': \widehat{f}(\mathbf{y}'|\mathbf{x}) \geq \widehat{f}(\mathbf{y}|\mathbf{x})} \widehat{f}(\mathbf{y}'|\mathbf{x}) d\mathbf{y} \quad (6)$$

$$= \int_{\mathbf{y}': f(\mathbf{y}'|\mathbf{x}) \geq f(\mathbf{y}|\mathbf{x})} f(\mathbf{y}'|\mathbf{x}) d\mathbf{y}. \quad (7)$$

Applying the results about uniformity of HPD for $f(\cdot|\mathbf{x})$ from Harrison et al. [2015, Section A.2] (also reproduced in the proof of Theorem 4) proves the theorem. □

K	2	3	4	5	6	7	8	9	10
KL loss	-0.729	-0.885	-0.915	-0.906	-0.897	-0.917	-0.906	-0.911	-0.905

Table 1: The KL divergence loss indicates that the number of mixture components in the ConvMDN approximation of the posterior in Example 2 should be $K = 7$.

B: EXAMPLE 1: OMITTED VARIABLE BIAS IN CDE MODELS

Figure 6, right panel, shows the p-values from LCTs across the feature space for the model \hat{f}_2 . Unlike model \hat{f}_1 , which was fit on X_1 solely, \hat{f}_2 was fit on both X_1 and X_2 variables. Hence, \hat{f}_2 is able to pass all tests, with local P-P plots indicating a good fit (with two examples shown in the Figure 6, left panel).

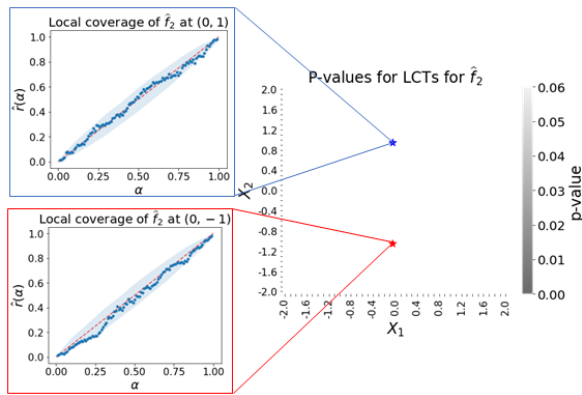


Figure 6: P-values for LCTs for \hat{f}_2 in Example 1 suggest an adequate fit everywhere in the feature space; local coverage plots at selected points also suggest a good fit.

C: EXAMPLE 2: POSTERIOR INFERENCE FOR SYNTHETIC GALAXY IMAGES

Table 1 reports the KL divergence loss over a test set of 1000 galaxy images for a ConvMDN model with K components, for $K = 2, \dots, 10$. However, the model which minimizes the KL loss (a ConvMDN with $K = 7$ components) fails to pass our GCT and is therefore not a good approximation of the true conditional density. We can use LCTs and P-P plots to diagnose the inadequacies in the fit (Figure 5).